Supporting Information

Reduced ice adhesion using amphiphilic Poly (Ionic Liquid)-based surfaces

Zahra Mossayebi [†,‡], *Vianna F. Jafari*[†], *Paul A. Gurr*[†], *Ranya Simons*[*,‡], *Greg G. Qiao*[*,†]

[†] Department of Chemical Engineering, The University of Melbourne, Melbourne, Victoria 3010, Australia

[‡] CSIRO Manufacturing, Melbourne, Victoria 3169, Australia

[*]Email: Ranya.Simons@csiro.au
[*]Email: gregghq@unimelb.edu.au

1. Experimental Section

1.1 Materials

Bis(hydroxyethyloxypropyl) polydimethylsiloxane (HO-PDMS-OH, DMS-C23, 300-350 cSt) were supplied from Gelest. N,N-Dicyclohexylcarbodiimide (DCC, 99%), N,N-Dimethylpyridin-4-amine (DMAP, 99%), bromobenzene (> 99.5%), magnesium (> 99%), carbon disulphide (anhydrous, > 99%) potassium hexacyanoferrate(III), 4,4'-Azobis(4-cyanopentanoic acid) (ABCVA, > 98%), [2-(methacryloyloxy)ethyl]trimethylammonium chloride solution (METAC, 80 wt.% in H_2O), Lithium bis(trifluoromethanesulfonyl)imide (LiTFSI), Oligoethylene glycol dimethacrylate (OEGDMA, M_n ~ 300 g mol^{-1}, 98%), 2-Hydroxy-4′-(2-hydroxyethoxy)-2-methylpropiophenone (Irgacure 2959, 98%) were all purchased from Sigma-Aldrich. 4-Cyanopentanoic acid dithiobenzoate (CPADB) was synthesized according to the literature.[1-5] 2, 2′-Azobis-(isobutyronitrile) (AIBN) was recrystallized from methanol three times before use. Solvents of anhydrous dichloromethane (DCM) and tetrahydrofuran (THF) were vacuum distilled before any usage. Aluminium panels (aircraft grade 2024-T3, 50 × 50 mm^2, 1 mm thick) were purchased locally by CSIRO manufacturing sector. Unless otherwise noted, all the other chemicals were obtained from Sigma-Aldrich and used as received without further purification. Wearlon™ Super F-1 anti-icing coating, industrial coating control, was purchased from Plastic Maritime Corporation. SYLGARD™ 184 (Dow Corning), a siloxane-based control coating, was prepared following the procedure described elsewhere (base:curing agent (10:1), curing temperature/duration (80 ℃ / 2 h)).[7]

1.2 Synthesis

Synthesis of 4-cyanopentanoic acid dithiobenzoate (CPADB) RAFT agent

In an oven-dried two-neck round-bottom flask containing a stirrer bar equipped with a condenser, magnesium (2g, 82.3 mmol), anhydrous THF (80 mL) and a small amount of Iodine were added under an argon atmosphere, respectively. Bromobenzene (11.175g, 71.2 mmol) was added dropwise and the mixture was stirred at 70 ℃ for 3 h. The resulting grey solution was cooled down to 0 ℃ and carbon disulphide (6.1 g, 80 mmol) was added dropwise to the Grignard mixture. The solution was stirred for 1.5 h at 0 °C before stirring at room temperature for 1 h. The mixture was quenched by the slow addition of a mixture of ice and water (10 ml). The magnesium salts were removed by filtration and washed with water. The solution was transferred to a 1L separating funnel and 1.0 N HCl solution (130 ml) was added. The pink organic phase was separated, and the aqueous phase was washed with Diethyl ether (3 × 150 mL). The combined organic layers were washed with a 1.0 N NaOH solution (150 ml) to transfer dithiobenzoate into the aqueous phase. The dark red aqueous layer was further washed with Diethyl ether (2 × 150 mL), leaving a dark red solution of the sodium salt of dithiobenzoic acid. The solution of the sodium dithiobenzoate was placed in 1L round-bottom

flask equipped with an addition funnel, and a reflux condenser. A solution of potassium hexacyanoferrate(III) (24 g, 73 mmol) in 100 mL distilled water was added dropwise to the vigorously stirring solution, over 1.5 h. The red precipitate was washed and collected by vacuum filtration and dried under the high vacuum to give the resulting di(thiobenzoyl) disulphide (9.99 g, 91.6% yield), in agreement with previous literature [1, 3-4, 8]. **^{1}H NMR** (500 MHz, $CDCl_3$): δ 7.46 (m, 4H), 7.61 (m, 2H), 8.08 (m, 4H). **^{13}C NMR** (125 MHz, $CDCl_3$): δ 127.50, 128.58, 133.09, 143.61, 219.50.

For the synthesis of CPADB RAFT agent, 4,4'-Azobis(4-cyanopentanoic acid) (ABCVA) (5.84 g, 21 mmol) and di(thiobenzoyl) disulphide (4.25 g, 14 mmol) were dissolved in dry ethyl acetate (80 ml). The reaction solution was refluxed for 18h before ethyl acetate was removed under reduced pressure. The product was isolated by flash column chromatography (EtOAc/Hex, 3.5:6.5), which was further purified using crystallization over EtOAc/Hex to yield the red crystals (5.3 g, 67.75 % yield). The above synthetic procedure is according to the literature [1, 3-4, 8-9]. **^{1}H NMR** (500 MHz, CDCl3) δ1.94 (s, 3H), 2.73–2.46 (m, 4H), 7.40 (m, 2H), 7.57 (m, 1H), 7.90 (m, 2H). **^{13}C NMR** (125 MHz, CDCl3) δ 24.6, 29.9, 33.4, 46.0, 118.8, 127.1, 129, 133.5, 144.9, 177.7, 222.5. **FTIR:** 3032-2820 cm^{-1} (C–H stretching of aromatic and aliphatic), 2231 (–CN stretching), 1705 cm^{-1} (C=O stretching), 1380–1455 cm^{-1} (C–H bending), 1049 cm^{-1} (C=S stretching), 764 cm^{-1} (γ(C–H) in the aromatic ring), 690 cm^{-1} (C–S stretching).

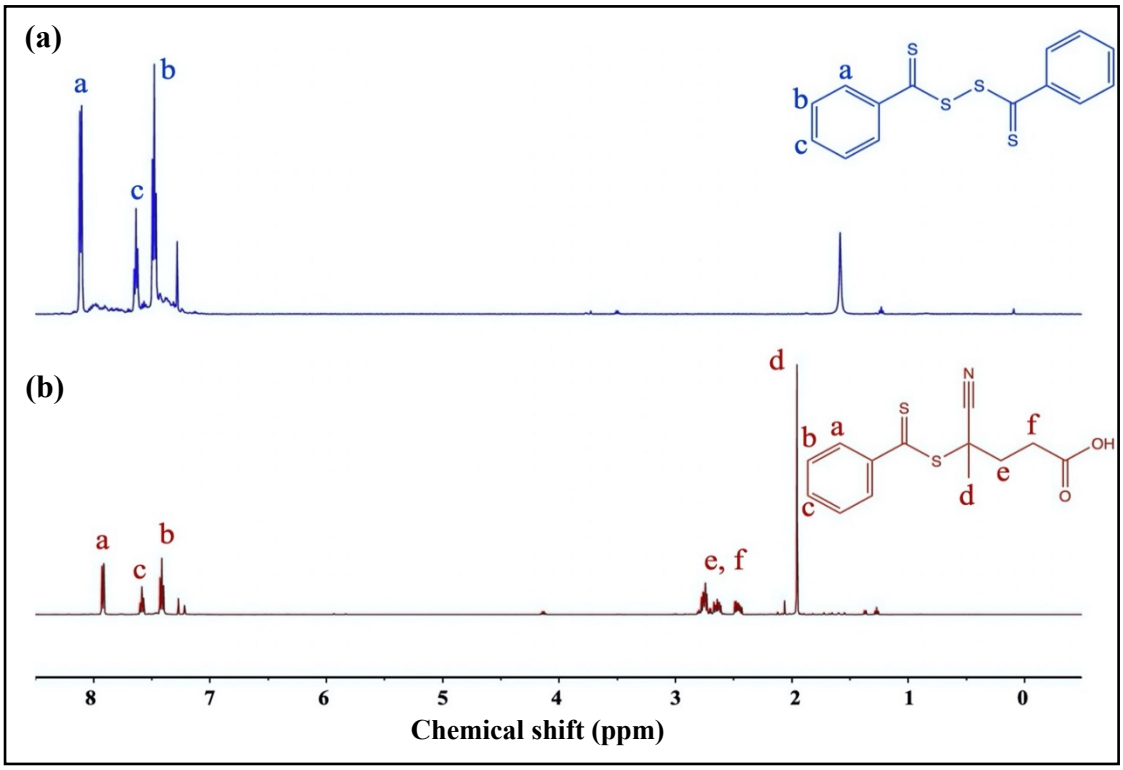

Figure S1. ^{1}H NMR spectra of the synthesized (a) Di(thiobenzoyl) Disulfide, and (b) CPADB RAFT agent, in $CDCl_3$.

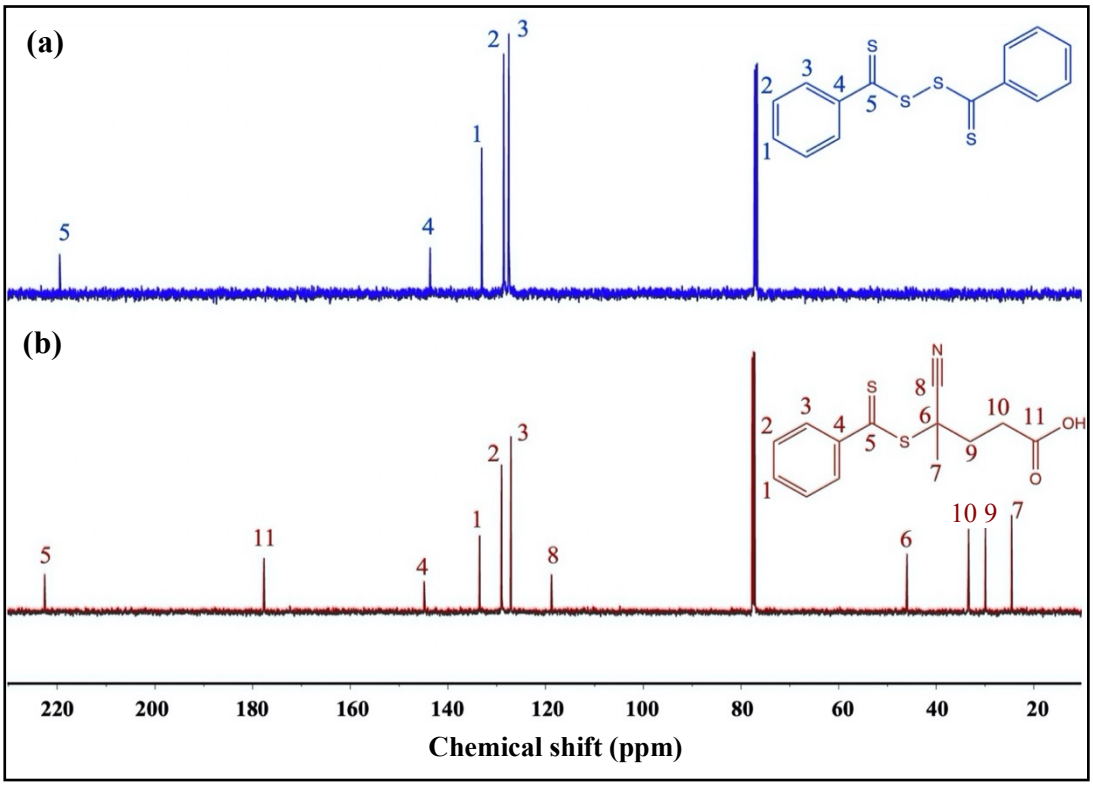

Figure S2. ^{13}C NMR spectra of the synthesized (a) Di(thiobenzoyl) Disulfide, and (b) CPADB RAFT agent, in $CDCl_3$.

Synthesis of PDMS-based RAFT macro-initiator

HO-PDMS-OH (10 g, 1.0 mmol), CPADB (0.84 g, 3.0 mmol), DCC (0.70 g, 4.5 mmol) and DMAP (0.12 g, 0.90 mmol) were added to a round-bottom flask and dried under reduced pressure overnight. Anhydrous CH_2Cl_2 (50 mL) was added and the reaction mixture was stirred at 0 ºC for 10 h followed by 20 h at room temperature under an argon atmosphere. The reaction mixture was then filtered, and the filtrate was concentrated under reduced pressure. The crude product was precipitated (× 3) in methanol and dried under vacuum for 24 h. The CTA-PDMS-CTA was obtained as a red oily liquid (7.81 g, 78.1% yield) that is in agreement with the literature.[10-12] **FTIR**: 2960–3020 cm^{-1} (C–H stretching), 1744 cm^{-1} (C=O stretching), 1258 (CH_3 symmetric bending), 1080 cm^{-1} (C–O and Si–O–Si stretching), 789 cm^{-1} (Si–C stretching).**^{1}H NMR** (500 MHz, $CDCl_3$, δ): 0-0.2 (m, (6n + 12)H), 0.55 (m, 4H), 1.63 (m, 4H), 1.94 (s,6H), 2.18–2.76 (m, 4H), 3.44 (m, 4H), 3.65 (t, 4H), 4.26 (t, 4H), 7.41 (m, 2H), 7.58 (m, 1H), 7.91 (m, 2H), $M_{n,GPC}$ = 13.7 kDa, PDI = 1.58.

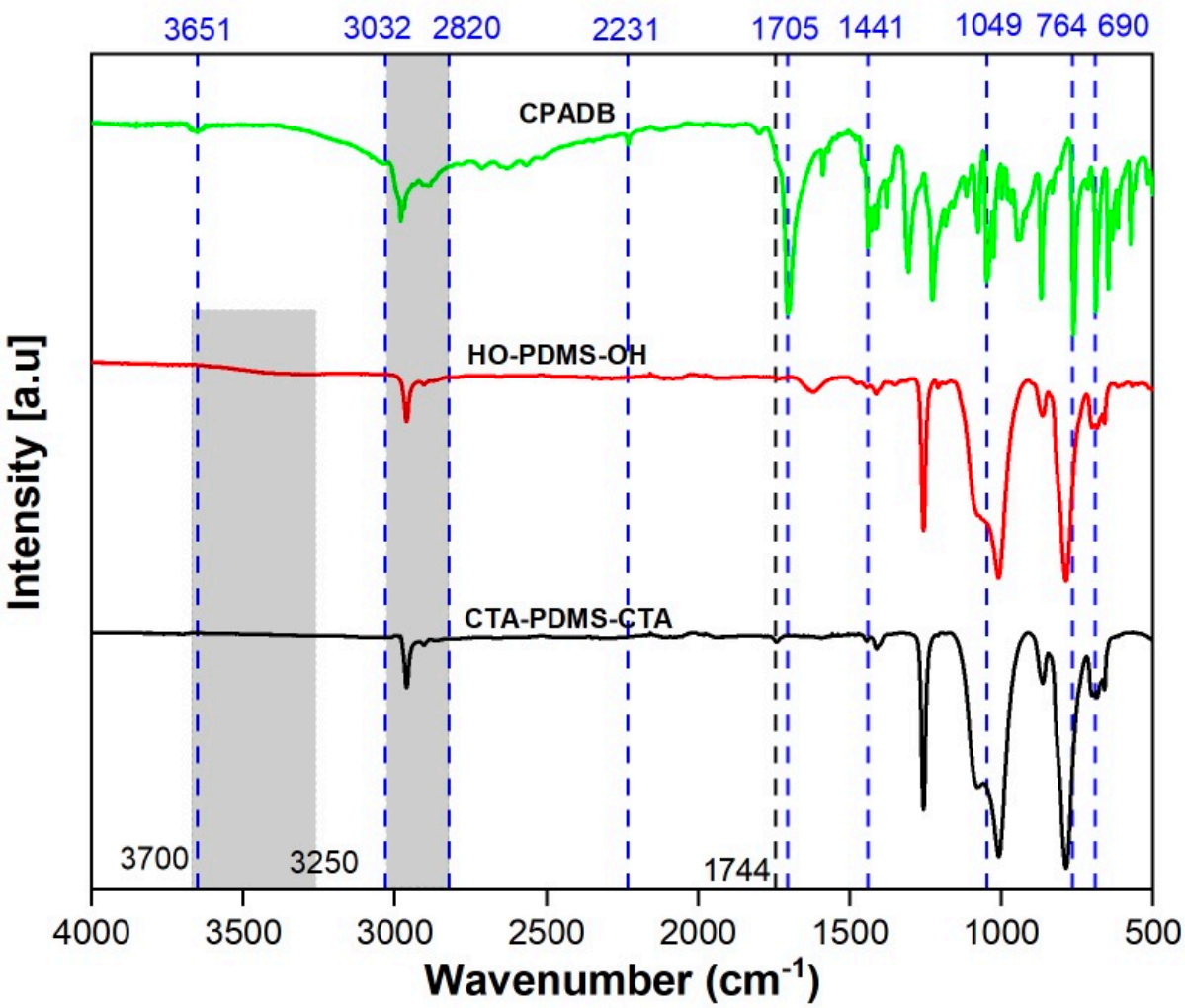

Figure S3. FTIR spectra of the 4-Cyanopentanoic acid dithiobenzoate (CPADB) RAFT agent, bis(hydroxyethyloxypropyl) polydimethylsiloxane (HO-PDMS-OH), and PDMS-RAFT macroinitiator (CTA-PDMS-CTA).

Counterion exchange of [2-(Methacryloyloxy)ethyl] trimethylammonium chloride (METAC) with bis(trifluoromethanesulfonyl)imide (TFSI)

Li^+ $TFSI^-$ salt and METAC monomer (molar ratio of 1:2) were diluted with deionized water and stirred for 24 h at room temperature to induce liquid-liquid phase separation. The organic layer containing the monomer of [2-(methacryloyloxy)ethyl] trimethylammonium bis(trifluoromethanesulfonyl)imide (METAT) was isolated with a separating funnel and diluted with CH_2Cl_2. The organic layer was further washed with water (× 3) and dried under reduced pressure. **FTIR**: 1719 cm^{-1} (C=O stretching), 1639 cm^{-1} (C=C stretching), 1481 (CH_2 bending), 1344 cm^{-1} (vibrational $(SO_3)_a$), 1181 cm^{-1} (vibrational $(CF_3)_s$), 1134 cm^{-1} (C–N stretching), 1050 cm^{-1} (C–O stretching), 950 cm^{-1} (C–H vibration of quaternary), 790 cm^{-1} (vibrational (C–S) + vibrational (S–N)), 740 cm^{-1} (vibrational (S–N)) . **^{1}H NMR** (500 MHz, CD_3COCD_3, δ): 1.93 (s, 3H), 3.49 (s, 3H), 4.03 (t, 2H), 4.74 (t,2H), 5.71(s, 1H), 6.13 (s, 1H). **^{19}F NMR** (470 MHz, CD_3COCD_3, δ): –79.93 (–CF_3).

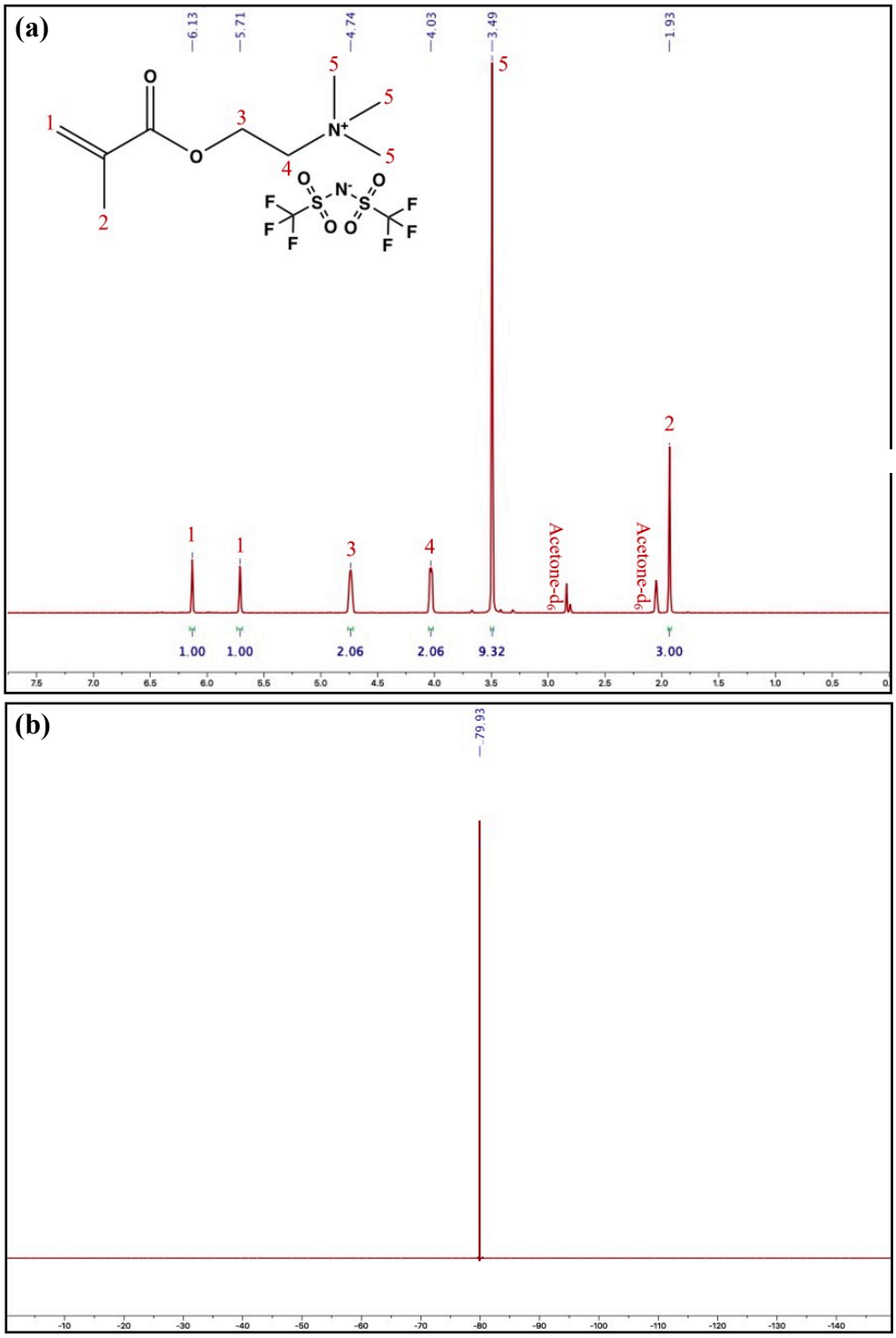

Figure S4. (a) ^{1}H NMR and, (b) ^{19}F NMR spectra of [2-(Methacryloyloxy)ethyl] trimethylammonium bis(trifluoromethanesulfonyl)imide (METAT) in acetone-d_6.

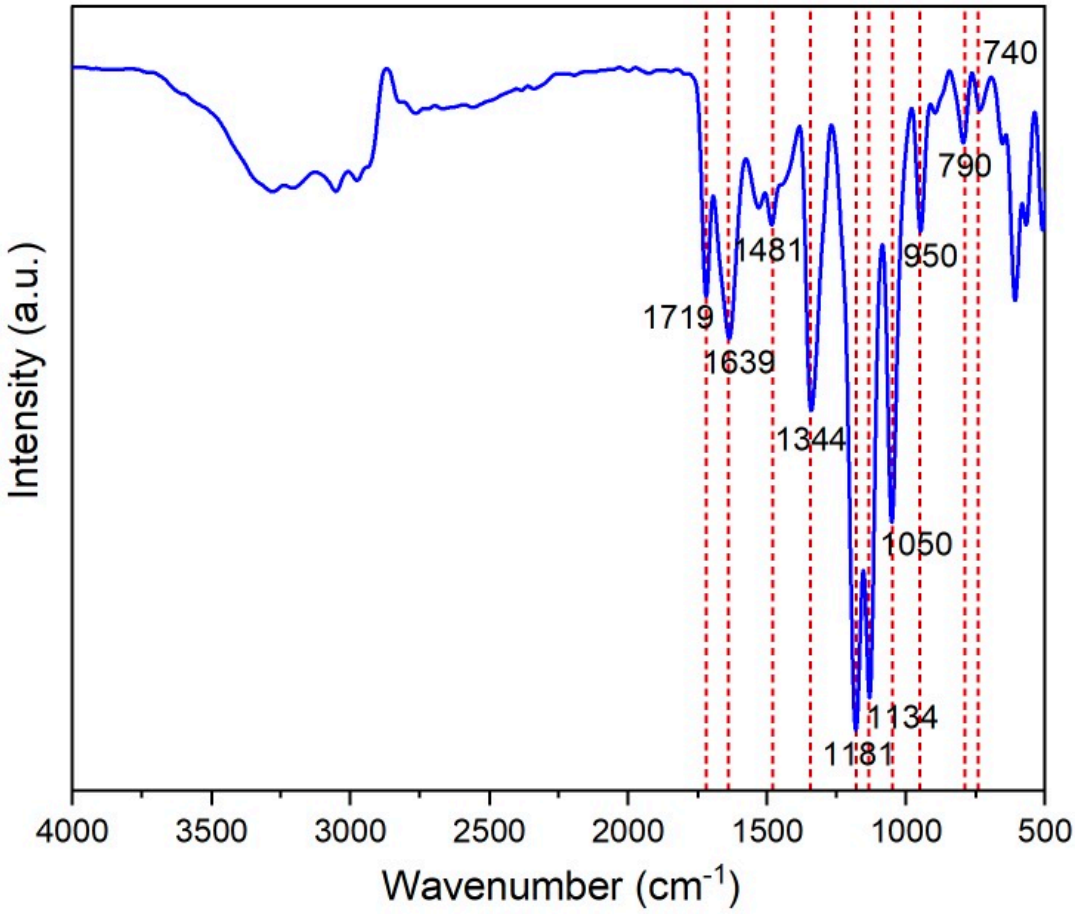

Figure S5. FTIR spectra of [2-(Methacryloyloxy)ethyl] trimethylammonium bis(trifluoromethanesulfonyl)imide (METAT).

Preparation of triblock copolymers and corresponding coatings

In a typical experiment for the synthesis of SAT12, CTA-PDMS-CTA (1.21 g, 0.092 mmol), METAT (0.50 g, 1.105 mmol) and AIBN (0.003 g, 0.018 mmol) were dissolved in the mixture of 1,4-Dioxane: THF (4:1, 7.5 mL) in a round-bottom flask and deoxygenated using argon gas for 30 min at room temperature. The sealed reaction vessel was stirred for 24 h at 70 ºC. The reaction mixture was precipitated in methanol (× 3) and vacuum dried at 65 ºC overnight to yield a light pink solid product. For the synthesis of SACx triblocks, the same synthetic procedure was employed with followed changes: the solvent mixture to 1,4-Dioxane: ethanol (1.5:1), polymerization time to 12 h and precipitation in diethyl ether (for x = 25, 50).

For fabrication of the PIL-based coatings, the triblock copolymers were dissolved in appropriate solvents (ethanol for SACx and THF for SATx) at a concentration of 30 wt.%. Irgacure 2959 (0.4 wt.% in final solution) and varied contents of OEGDMA (2.5 and 5 wt.% relative to the triblock copolymer) were added to the homogeneous copolymer solutions. The solution was spin-coated on the polished aluminium substrates (600 rpm for 6 s followed by 3000 rpm for 10 s) and cured under UV irradiation (365 nm, 36 W) for 3 h. For SAC12-based coatings, the irradiation time increased to 12 h. The resultant coatings dried at room temperature for 2 days followed by a vacuum-drying at 65 ºC overnight. The thickness of the films was estimated to be ~ 10-15µm.

1.3 Characterizations

Instrumental characterization

Proton (^{1}H), Carbon (^{13}C) and Fluorine (^{19}F) Nuclear Magnetic Resonance (NMR) spectroscopic analysis was performed on an Agilent 500 MHz spectrometer.

Attenuated total reflection- Fourier transform infrared (ATR-FTIR) spectroscopy was carried out using a Bruker Tensor 27 FTIR, with a GladiATR ATR attachment obtained from Pike Technologies.

Gel permeation chromatography (GPC) was performed on a Waters Alliance system equipped with an Alliance 2695 Separations Modul, a Waters column heater module, a Waters 2414 RDI refractive index detector, a Waters PDA 2996 photodiode array detector and 4 × Agilent PL-Gel columns. THF was used as an eluent with a flow rate of 1 mL/min at 30 °C. Number (M_n) and weight average (M_w) molar masses were evaluated using Waters Empower-3 software. The GPC columns were calibrated with low dispersity polystyrene (PSt) standards.

Scanning electron microscope (SEM) images and Energy-dispersive X-ray (EDX) elemental mappings (e-beam voltage = 15 keV) were acquired using a Hitachi FlexSEM 1000 microscope. Atomic force microscope (AFM) images of the films were obtained under tapping mode on an Asylum Research Cypher machine.

The measurement of static and dynamic contact angles was performed on a Dataphysics OCA 20 tensiometer. For measurement of contact angle hysteresis (CAH), which is the difference between the advancing and receding contact angles, the needle-in-the-sessile-drop method was used by softly settling a 5 µL water droplet on the surface and then delicate sucking of 4 µL water from the droplet into the syringe.[13] The surface energies of the films were calculated according to the Fowkes model[14] by measuring the static contact angles of water and diiodomethane on the surface.

Anti-icing tests

The ice adhesion strength of the coated substrates was measured utilizing an Instron Universal Testing Machine in tensile mode and performed in an environmental chamber at – 20 ºC to simulate freezing conditions (**Figure S6**). Before conducting the test, the stainless-steel cuvettes were placed on the coated substrates and the assembly was left inside a deep freezer at – 20 ºC overnight to reach equilibrium. Deionized water (4 ml) was then poured into the cuvettes and was frozen for 4 h prior to the ice adhesion measurement. The device was equipped with a fan/refrigerator that provides a well-controlled subzero temperature within the chamber with a precise cooling rate. The test involved placing samples into a removable stainless-steel sample holder and the position of the coated substrate was fixed for an accurate measurement. The force was then gradually applied and the maximum load (N) and maximum tensile stress (MPa) recorded as a measure of ice adhesion.

Hydration / de-hydration studies

Differential Scanning Calorimetry (DSC) analysis, to study the hydration states of the coatings, were carried out according to the literature [15-18] using a Perkin Elmer instrument (DSC 8500) and

Pyris™ software platform. A coating/water binary system was prepared by the addition of 150 $wt.\%$ of deionized water to the coatings which was scratched from the substrate and placed in aluminium pans. After 2 weeks of equilibration at ambient temperature, three cooling/heating cycles were performed on the sealed samples by cooling down the temperature from 20 ºC to – 50 ºC holding for 3 min, and then heating up to 20 ºC at the rate of 5 ºC/min. Cooling cycles provided information on the depressing of the freezing point of water, while heating cycles were used to calculate the amount of water in different states in the coatings based on the following equations [16, 19]:

- Total water content (W_c): $W_c = m_w/m_c$ (m_w and mc represent the weights of the water and coating)
- Freezable water content (W_f): $W_f = A_c/(334m_c)$
  A_c (mJ) is the integral area of the melting peak in the heating curve vs. time obtained by thermal software, and 334 (J g^{-1}) is the specific heat of fusion of water.
- Non-freezable bound water content (W_{nfb}): $W_{nfb} = W_c - W_f$
- Freezable bound water content (W_{fb}): $W_{fb} = A_{c,fb} / (334m_c)$
  W_{fb} was calculated according to the area of the symmetric peak at the heating curve.
- Bound water content (W_b): $W_b = W_{nfb} + W_{fb}$
- Freezable free water content (W_{ff}): $W_{ff} = W_f - W_{fb}$

To measure the water evaporation rates of the coatings, the variations in the weight of the samples with time were recorded. The samples (50 × 50 mm^2) were kept under a RH of 50% at 37 ℃ in an incubator and weighed every 2 h until no significant variations determined. The following equation used to calculate the evaporation rate of water (W_0 , W_t , and W_d are, respectively, the initial weight, the weight at prescribed time and the final weight of the coatings):

$$\%\, Water\ lost = \frac{W_0 - W_t}{W_0 - W_d} \times 100$$

Figure S6. Ice adhesion test apparatus.

Mechanical tests

The tape peeling test was conducted following the standard test method B of ASTM D3359-09$^{\varepsilon 2}$ [20]. In brief, A lattice pattern with eleven cuts in each direction (1 mm apart, 20 mm long) was made on the film and a pressure-sensitive tape (3M, Scotch 600) was applied over the lattice and pressed using a rubber eraser. After 90 ± 30 s of application, the tape was quickly peeled off at an angle of 180 ° and the results were reported on a scale of 0B to 5B. In addition, the hardness of the coatings was measured per ASTM D3363 [21]. The pencils with various grades of hardness, from extremely hard (8H) to quite smooth (8B), moved across the coating at an angle of 45 °. The first pencil which did not scratch the surface was considered as the hardness of the coating. The Young's modulus of the coatings was estimated using an Asylum Research Cypher Atomic Force Microscope (AFM), in the force Mapping mode. A silicon probe with a visible apex tip for tapping mode and tip radius of 7 nm was employed and the spring constant of the cantilever was calibrated loading a clean silicon wafer substrate. By calibration of the InvOLS (Inverse Optical Lever Sensitivity) parameter and the subsequent thermal tuning, the resultant spring constant of 22 N m^{-1} was achieved. Next, force mapping measurement was performed on the immobilized coating samples to create an image of Young's modulus distribution of the surface, by acquiring a 10 ×10 array of force-distance curves on a 2 μm × 2 μm scan area. Each single force curve, corresponding to one pixel, was further analysed and fitted to the Johnson–Kendall–Roberts (JKR) model to give the value of Young's elastic modulus of that specific point, and the mean value was reported for the entire surface area of the coating, assigned to 100 pixels.

2. Supporting Figures for the Results and Discussion

2.1 Surface morphology of the fabricated coatings using Scanning Electron Microscopy (SEM)

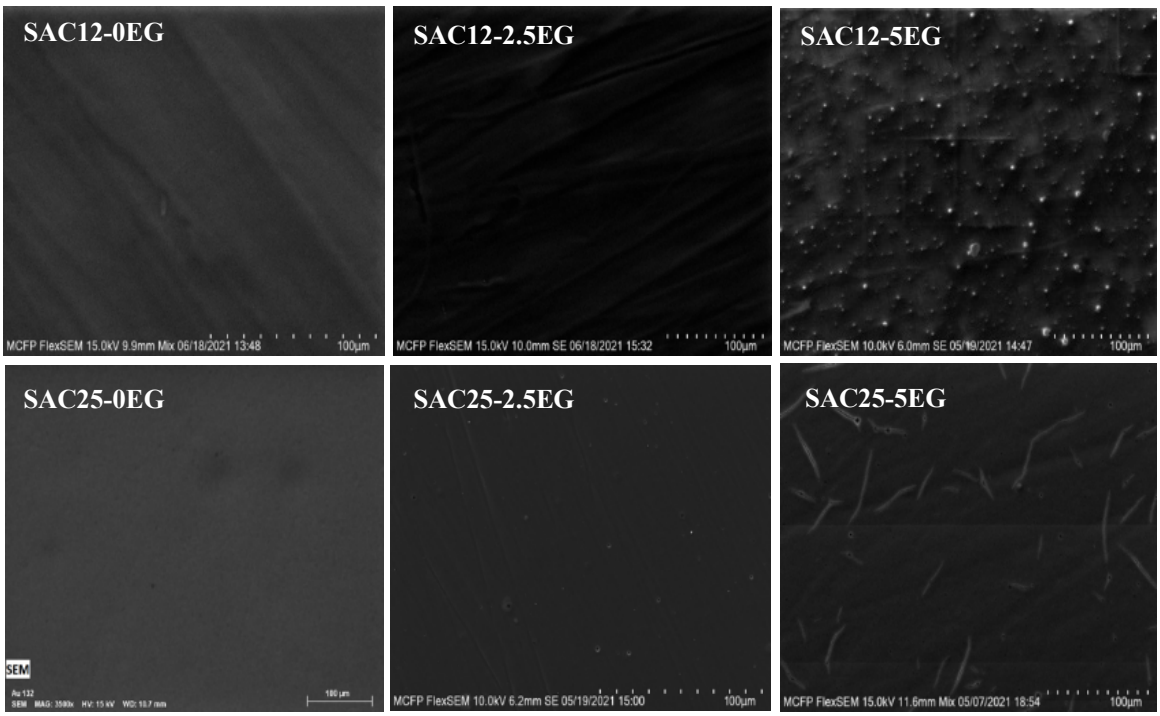

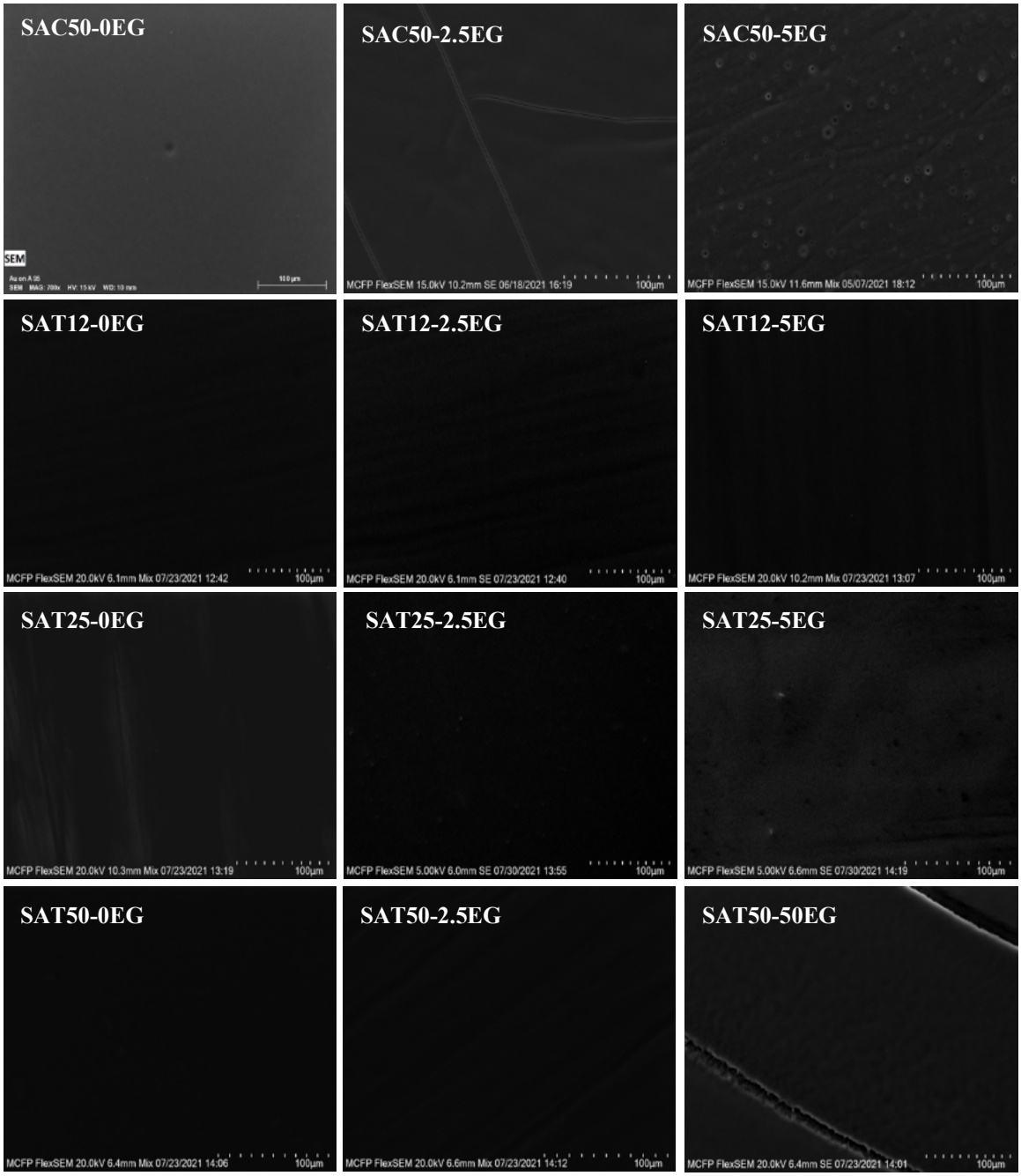

Figure S7. Scanning electron microscopy (SEM) images of the PIL-based fabricated coatings.

2.2 AFM phase images of the fabricated coatings

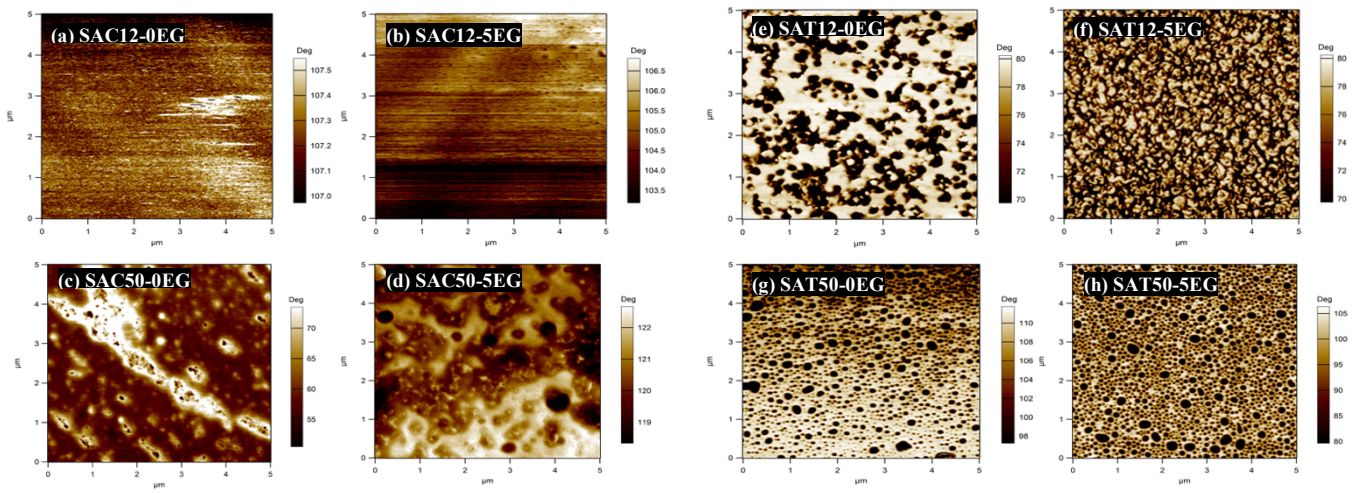

Figure S8. Tapping mode AFM phase images of the prepared coatings in air for a scan area of 5 µm × 5 µm. Each label shows the composition of the imaged coating.

2.2. Energy-dispersive X-ray (EDX) mappings of PIL-based surfaces

EDX elemental mappings of SA12-5EG and SAC50-5EG coatings complemented the AFM results on the distribution regularity of the coating components. Si and Cl are representative elements of PDMS and PMETAC, respectively.

Table S1. Surface element compositions of SAC12-5EG and SAC50-5EG SIPNs obtained by EDX analysis.

Sample	Element Compositions (atomic %)				Surface Cl/Si atomic ratio
	C	O	Si	Cl	
SAC12-5EG	48.4	21.62	21.15	0.52	0.026
SAC50-5EG	60.78	17.41	6.68	3.28	0.49

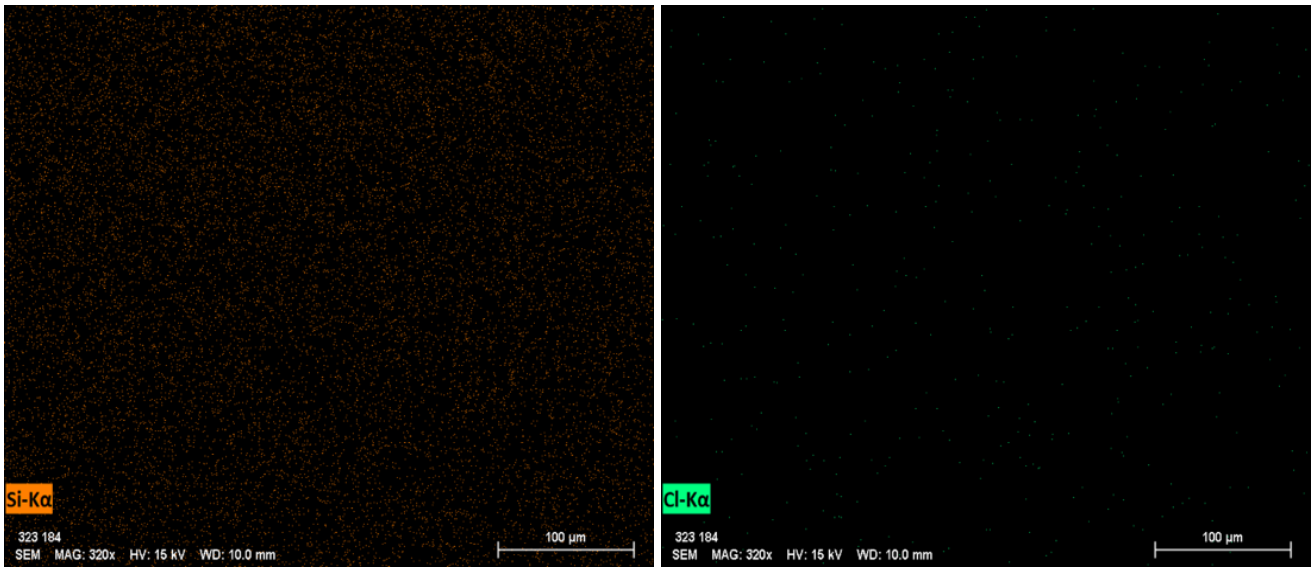

(a) SAC12-5EG

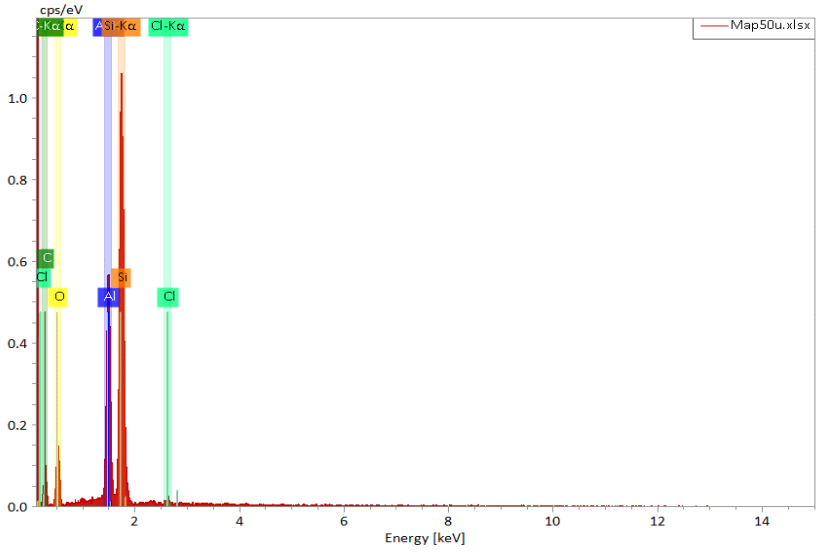

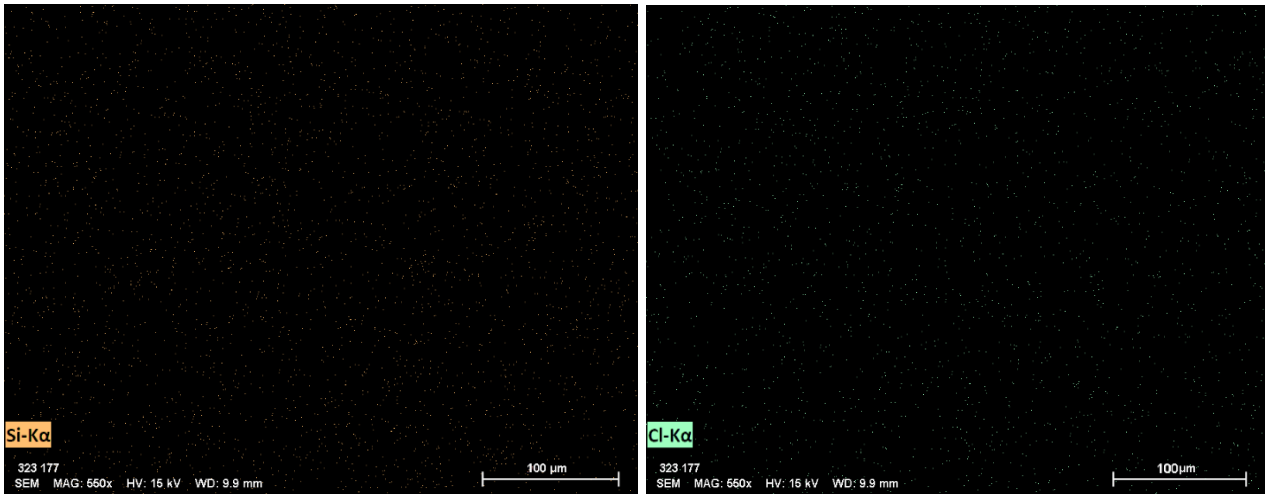

(b) SAC50-5EG

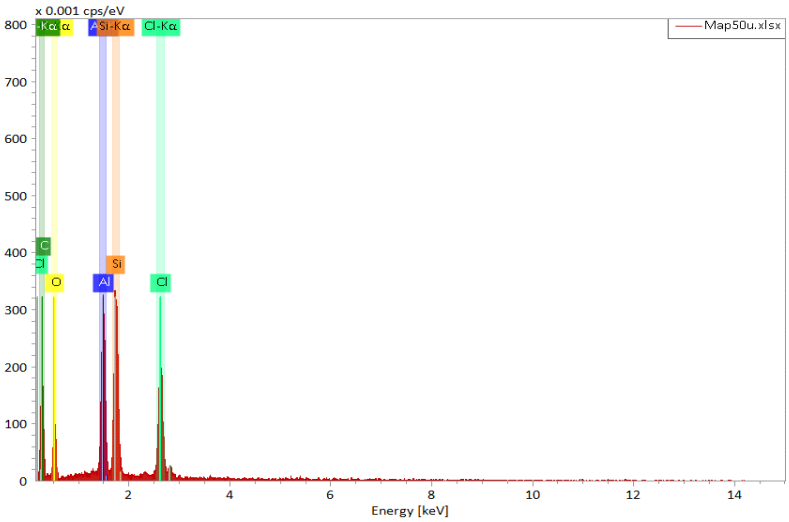

Figure S9. EDX-mapping of (a) SAC12-5EG, and (b) SAC50-5EG coatings along with the distribution of the silicon and chlorine elements over the surface.

2.3 Evolution of the water contact angle (WCA) on the SAC-based amphiphilic coating

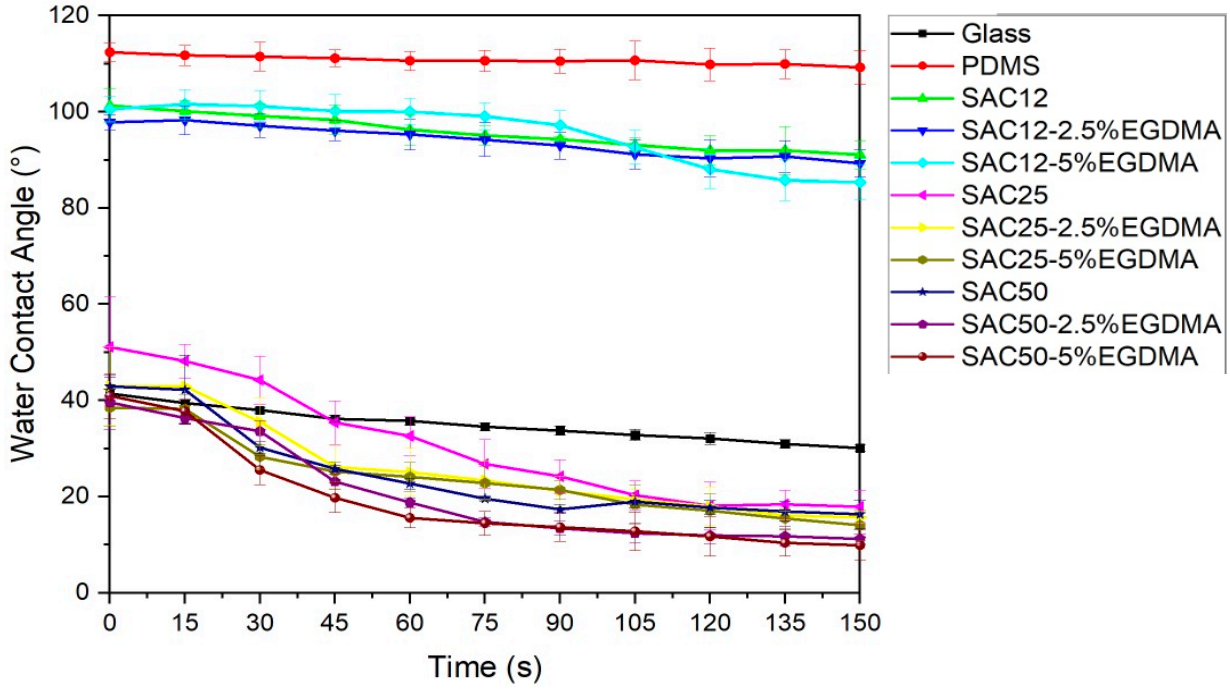

Figure S10. Evolution of the water contact angle (WCA) in the SAC-based coatings.

2.4 Hydration / de-hydration analysis of the SAC-based coatings

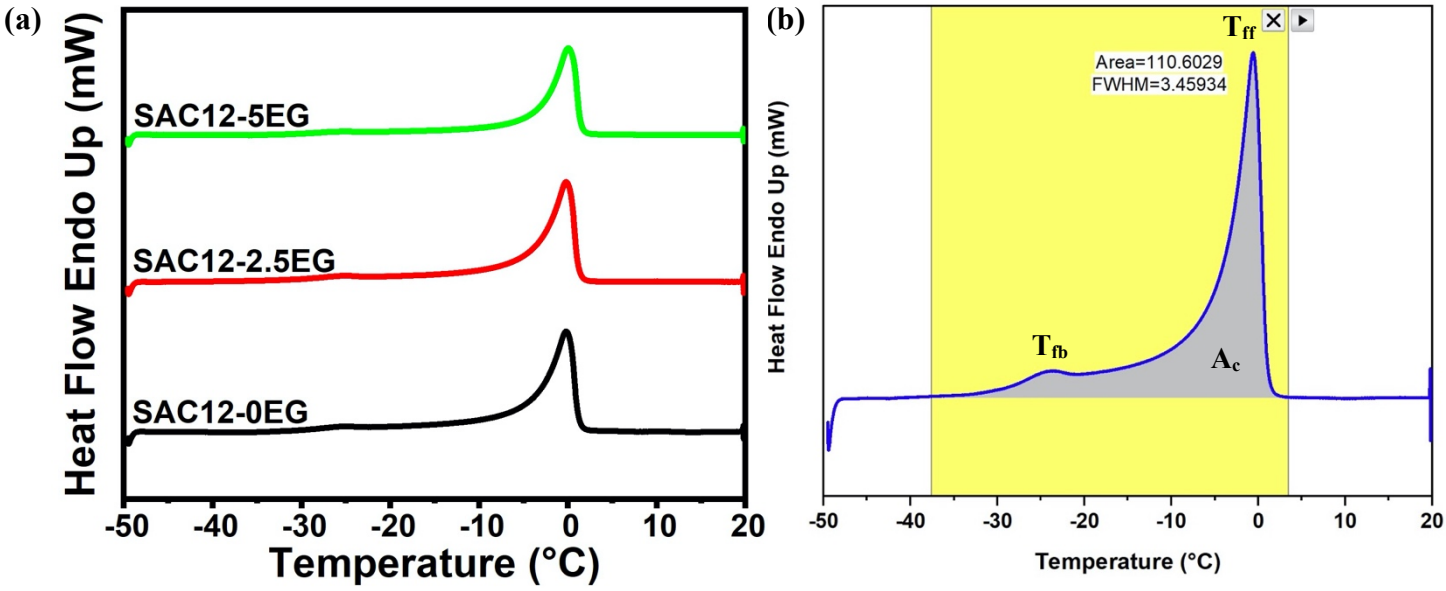

Figure S11. DSC heating scans of (a) SAC12-based coatings at a heating rate of 5 °C/min., and (b) SAC12-5%OEGDMA/water binary system and peak integrating via origin 8.0.

As shown in **Figure S12**, DSC heating curves of SAC12-5EG/water binary system with different water contents (W_c) were analyzed. It can be observed that the DSC heating trace is absent of a melting endotherm at 0.15 and 0.3 water content, indicating that all of the water is in a non-freezable state. When there is 0.8 or more water in this coating, two small melting endotherms are observed, presumably due to the freezable bound water and free water, respectively, and the free water becomes dominant, the melting temperature of which increases with the water content. These results suggested that the threshold for the amount of the W_{nfb} in this coating could be above 0.3. On the other hand, it was found that W_{nfb} was 0.31 when W_c = 0.8 and the contents of W_{nfb} (around 0.3) were almost the same when W_c increased from 0.8 to 1.5, while W_{fb} increased from 0.096 (W_c = 0.8) to 0.17 (W_c= 1.5). So, it is suggested that for this coating the W_{nfb} should be around 0.3 and this test can confirm the reliability of the DSC measurements.

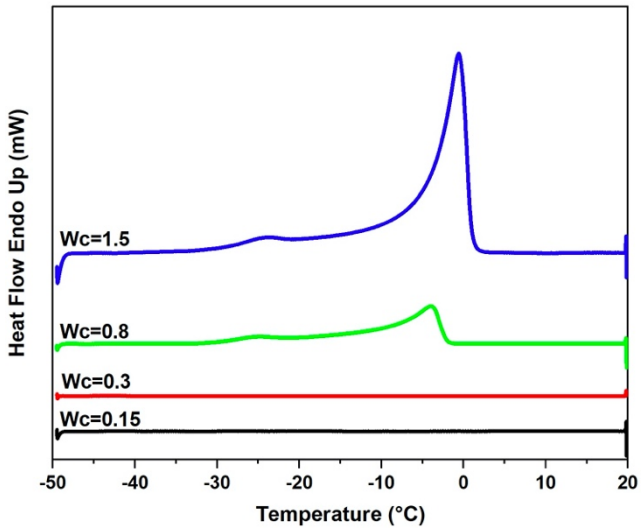

Figure S12. DSC heating scans of the SAC12-5EG coating containing different contents of W_c.

The water evaporation rates of the coatings are illustrated in Figure S13. A rapid loss of water for all coatings within the initial 10-12 h is indicated followed by no significant evaporation till 24 h. Semi-interpenetrating polymer networks showed slightly higher evaporation rates compared to those without OEGDMA crosslinker. The water loss reached to about 65% in SAC25-based and SAC50-based coatings while SAC12-based coatings lost no more than ca. 35%. However, all the coatings showed excellent capability for the self-replenishment of water as an increase in their weights was observed after being stored at higher humidity (RH: 80%).

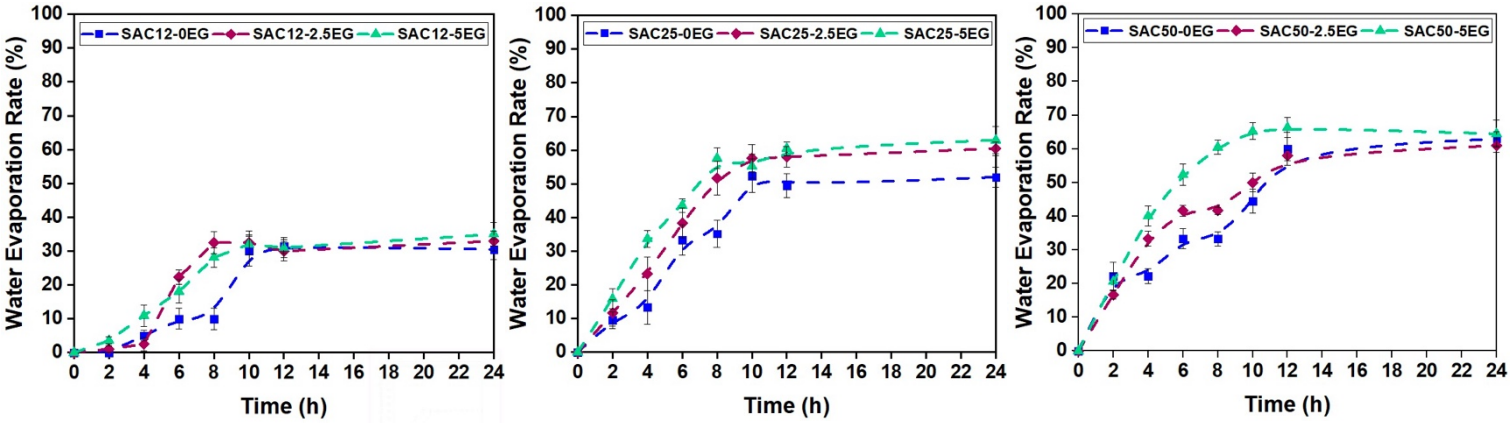

Figure S13. Water evaporation rate of: (a) SAC12-based, (b) SAC25-based, and (c) SAC50-based coatings.

2.5. Comparison of the ice adhesion strength of the developed IL-based surfaces in the literature

Table S2. Summary of the ice adhesion strength and other anti-icing results of the developed IL-based surfaces in the literature.

Coating composition	Ice adhesion strength (kPa)	Other results	Type of the coating	Ref.
Cationic [2-(methacryloyloxy)ethyl]-trimethylammonium chloride] and anionic [poly(3-sulfopropyl methacrylate), poly(sodium methacrylate)] polyelectrolyte brushes	The lowest value: G-SO_3^- Li^+ **320 kPa** at – 18 °C	-	polyelectrolyte brush	[22]
Cationic poly[2-(methacryloyloxy)-ethyltrimethylammonium] (PMETA) and anionic poly(3-sulfopropylmethacrylate) (PSPMA) brushes	-	Delay in ice nucleation	polyelectrolyte brush	[23]
Cationic poly[2-(methacryloyloxy)-ethyltrimethylammonium] (PMETA) brushes	-	Delay in ice nucleation and propagation	polyelectrolyte brush	[24]
P(DMAEMA-co-FMA)-b-polyelectrolytes	-	Antifogging Frost resisting	Amphiphilic IL-based	[16]
Poly(acrylamide-co-acrylic acidco-N-allylacrylamide) (poly(AAm-co-AAc-co-AAene))-*co*-PDMS-*g*-PMETA	**20 kPa** at – 10 °C to – 40 °C	Delay in ice nucleation and propagation	Hydrogel	[25]
1-butyl-3-methylimidazolium bromide (BMImBr) -Gelatin	Reduction in ice adhesion (no value reported)	Delay in ice nucleation and growth	Ionogel	[26]
1-octyl-3-methylimidazolium tetrafluoro-borate ([OMIM]BF_4) as the lubricant into polyurethane	**10.03 ± 2.62 kPa** at – 20 °C	Delay in ice nucleation	ILISs	[27]
PDMS-b-$(PMETAC)_2$ + 5 wt.% OEGDMA (SAC12-5EG)	**13.3 ± 8.6 kPa at – 20 °C**	**-**	**Amphiphilic IL-based**	**This work**

2.6. Mechanical strength of the PIL-based icephobic coatings

Table S3. Results of the pencil hardness test (ASTM D3363) and adhesion test (ASTM D3359) of the prepared coatings.

Coating Designation	Tape Peeling Test		Pencil Hardness
	Percent Area removed (%)	Classification	
SAC12-0EG	35 – 65	1B	8B
SAC12-2.5EG	15 – 35	2B	8B
SAC12-5EG	5 – 15	3B	6B
SAC12-10EG	5 – 15	3B	6B
SAC25-0EG	0	5B	5B
SAC25-2.5EG	0	5B	5B
SAC25-5EG	0	5B	5B
SAC50-0EG	0	5B	5B
SAC50-2.5EG	0	5B	5B
SAC50-5EG	0	5B	5B
SAT12-0EG	Less than 5	4B	6B
SAT12-2.5EG	0	5B	6B
SAT12-5EG	0	5B	6B
SAT25-0EG	Less than 5	4B	6B
SAT25-2.5EG	0	5B	6B
SAT25-5EG	0	5B	6B
SAT50-0EG	Less than 5	4B	6B
SAT50-2.5EG	0	5B	6B
SAT50-5EG	0	5B	6B

Supporting References

(1) Ye, Y.-S.; Shen, W.-C.; Tseng, C.-Y.; Rick, J.; Huang, Y.-J.; Chang, F.-C.; Hwang, B.-J. Versatile grafting approaches to star-shaped POSS-containing hybrid polymers using RAFT polymerization and click chemistry. *Chemical Communications* **2011,** *47* (38), 10656-10658.
(2) Hakobyan, K.; Gegenhuber, T.; McErlean, C. S.; Müllner, M. Visible-light-driven MADIX polymerisation via a reusable, low-cost, and non-toxic bismuth oxide photocatalyst. *Angewandte Chemie International Edition* **2019,** *58* (6), 1828-1832.
(3) Tochwin, A.; El-Betany, A.; Tai, H.; Chan, K. Y.; Blackburn, C.; Wang, W. Thermoresponsive and reducible hyperbranched polymers synthesized by RAFT polymerisation. *Polymers* **2017,** *9* (9), 443.
(4) Mitsukami, Y.; Donovan, M. S.; Lowe, A. B.; McCormick, C. L. Water-soluble polymers. 81. Direct synthesis of hydrophilic styrenic-based homopolymers and block copolymers in aqueous solution via RAFT. *Macromolecules* **2001,** *34* (7), 2248-2256.
(5) Ghamkhari, A.; Massoumi, B.; Jaymand, M. Novel 'schizophrenic'diblock copolymer synthesized via RAFT polymerization: poly (2-succinyloxyethyl methacrylate)-b-poly [(N-4-vinylbenzyl), N, N-diethylamine]. *Designed monomers polymers* **2017,** *20* (1), 190-200.
(6) Wang, Z.; Volinsky, A. A.; Gallant, N. D. Crosslinking effect on polydimethylsiloxane elastic modulus measured by custom-built compression instrument. *Journal of Applied Polymer Science* **2014,** *131* (22).
(7) Golovin, K.; Kobaku, S. P.; Lee, D. H.; DiLoreto, E. T.; Mabry, J. M.; Tuteja, A. Designing durable icephobic surfaces. *Science advances* **2016,** *2* (3), e1501496.
(8) Hakobyan, K.; Gegenhuber, T.; McErlean, C. S. P.; Mullner, M. Visible-Light-Driven MADIX Polymerisation via a Reusable, Low-Cost, and Non-Toxic Bismuth Oxide Photocatalyst. *Angew Chem Int Ed Engl* **2019,** *58* (6), 1828-1832, DOI: 10.1002/anie.201811721.
(9) Ghamkhari, A.; Massoumi, B.; Jaymand, M. Novel 'schizophrenic'diblock copolymer synthesized via RAFT polymerization: poly (2-succinyloxyethyl methacrylate)-b-poly [(N-4-vinylbenzyl), N, N-diethylamine]. *Designed monomers polymers* **2017,** *20* (1), 190-200.
(10) Li, X.; Zhang, K.; Zhao, Y.; Zhu, K.; Yuan, X. Enhancement of icephobic properties based on UV-curable fluorosilicone copolymer films. *RSC advances* **2015,** *5* (110), 90578-90587.
(11) Lopez-Oliva, A. P.; Warren, N. J.; Rajkumar, A.; Mykhaylyk, O. O.; Derry, M. J.; Doncom, K. E.; Rymaruk, M. J.; Armes, S. P. Polydimethylsiloxane-based diblock copolymer nano-objects prepared in nonpolar media via RAFT-mediated polymerization-induced self-assembly. *Macromolecules* **2015,** *48* (11), 3547-3555.
(12) Li, X.; Zhang, K.; Zhao, Y.; Zhu, K.; Yuan, X. Formation of icephobic film from POSS-containing fluorosilicone multi-block methacrylate copolymers. *Progress in Organic Coatings* **2015,** *89*, 150-159.
(13) Korhonen, J. T.; Huhtamäki, T.; Ikkala, O.; Ras, R. H. Reliable measurement of the receding contact angle. *Langmuir* **2013,** *29* (12), 3858-3863.
(14) Jie-Rong, C.; Wakida, T. Studies on the surface free energy and surface structure of PTFE film treated with low temperature plasma. *Journal of applied polymer science* **1997,** *63* (13), 1733-1739.
(15) Zigmond, J. S.; Pollack, K. A.; Smedley, S.; Raymond, J. E.; Link, L. A.; Pavía-Sanders, A.; Hickner, M. A.; Wooley, K. L. Investigation of intricate, amphiphilic crosslinked hyperbranched fluoropolymers as anti-icing coatings for extreme environments. *Journal of Polymer Science Part A: Polymer Chemistry* **2016,** *54* (2), 238-244.
(16) Bai, S.; Li, X.; Zhang, R.; Li, C.; Zhu, K.; Sun, P.; Zhao, Y.; Ren, L.; Yuan, X. Enhancing antifogging/frost-resisting performances of amphiphilic coatings via cationic, zwitterionic or anionic polyelectrolytes. *Chemical Engineering Journal* **2019,** *357*, 667-677.
(17) Bag, M. A.; Valenzuela, L. M. Impact of the hydration states of polymers on their hemocompatibility for medical applications: A review. *International journal of molecular sciences* **2017,** *18* (8), 1422.

(18) Heydari, G.; Tyrode, E.; Visnevskij, C.; Makuska, R.; Claesson, P. M. Temperature-dependent deicing properties of electrostatically anchored branched brush layers of poly (ethylene oxide). *Langmuir* **2016,** *32* (17), 4194-4202.
(19) Tao, C.; Bai, S.; Li, X.; Li, C.; Ren, L.; Zhao, Y.; Yuan, X. Formation of zwitterionic coatings with an aqueous lubricating layer for antifogging/anti-icing applications. *Progress in Organic Coatings* **2018,** *115*, 56-64.
(20) D3359-09 standard test methods for measuring adhesion by tape test. *ASTM International* **2009**, 1-5.
(21) D3363 Standard Test Method for Film Hardness by Pencil Test *ASTM International, West Conshohocken, PA* **2011**.
(22) Chernyy, S.; Järn, M.; Shimizu, K.; Swerin, A.; Pedersen, S. U.; Daasbjerg, K.; Makkonen, L.; Claesson, P.; Iruthayaraj, J. Superhydrophilic polyelectrolyte brush layers with imparted anti-icing properties: effect of counter ions. *ACS applied materials interfaces* **2014,** *6* (9), 6487-6496.
(23) He, Z.; Xie, W. J.; Liu, Z.; Liu, G.; Wang, Z.; Gao, Y. Q.; Wang, J. Tuning ice nucleation with counterions on polyelectrolyte brush surfaces. *Science advances* **2016,** *2* (6), e1600345.
(24) Liu, Z.; He, Z.; Lv, J.; Jin, Y.; Wu, S.; Liu, G.; Zhou, F.; Wang, J. Ion-specific ice propagation behavior on polyelectrolyte brush surfaces. *RSC advances* **2017,** *7* (2), 840-844.
(25) He, Z.; Wu, C.; Hua, M.; Wu, S.; Wu, D.; Zhu, X.; Wang, J.; He, X. Bioinspired multifunctional anti-icing hydrogel. *Matter* **2020,** *2* (3), 723-734.
(26) Zhuo, Y.; Xiao, S.; Håkonsen, V.; He, J.; Zhang, Z. Anti-icing ionogel surfaces: inhibiting ice nucleation, growth, and adhesion. *ACS Materials Letters* **2020,** *2* (6), 616-623.
(27) Wang, H. L.; Wang, Y. X.; Liang, Z. H.; Yang, H. C.; Xu, Z. K. J. A. M. I. Endogenous Ionic-Liquid-Infused Coatings by Phase Separation for Anti-Icing and Anti-Bacterial Applications. **2022,** *9* (13), 2102570.